

# A New Lower Main Sequence Eclipsing Binary with Detached Components\*

M. R o z y c z k a<sup>1</sup>, J. K a l u z n y<sup>1</sup>,  
P. P i e t r u k o w i c z<sup>1,2</sup>, W. P y c h<sup>1</sup>, B. M a z u r<sup>1</sup>,  
M. C a t e l a n<sup>2</sup> and I. B. T h o m p s o n<sup>3</sup>

<sup>1</sup>Nicolaus Copernicus Astronomical Center, ul. Bartycka 18, 00-716 Warsaw, Poland

e-mail: (mnr, jka, pietruk, pych, batka)@camk.edu.pl

<sup>2</sup>Departamento de Astronomía y Astrofísica, Pontificia Universidad Católica de Chile, Av. Vicuña Mackenna 4860, Macul, Santiago, Chile

e-mail: (pietruk, mcatelan)@astro.puc.cl

<sup>3</sup>The Observatories of the Carnegie Institution of Washington, 813 Santa Barbara Street, Pasadena, CA91101, USA

e-mail: ian@ociw.edu

## ABSTRACT

We present an analysis of NGC2204-S892 – a new detached eclipsing binary composed of two late K dwarfs. Based on three photometric campaigns launched in 2008 we obtained 5 light curves (3 in  $V$ , 1 in  $B$  and 1 in  $I$ ), and derived an orbital period of  $0.451780 \pm 0.000001$  d. We also obtained 20 VLT/UVES spectra, enabling accurate radial velocity measurements. The derived masses and radii of the components ( $m_1 = 0.733 \pm 0.005 M_\odot$  and  $R_1 = 0.72 \pm 0.01 R_\odot$ ;  $m_2 = 0.662 \pm 0.005 M_\odot$  and  $R_2 = 0.68 \pm 0.02 R_\odot$ ) are consistent with the empirical mass-radius relationship established recently for lower main sequence stars in binary systems; in particular we find that both stars are oversized compared to theoretical models. NGC2204-S892 is very active: both components show variable emission in  $H\alpha$  and  $H\beta$  and are heavily spotted, causing the light curve to show appreciable changes on a timescale of weeks. Our results add to the increasing evidence that the observed inflation of the radii of K and M stars is related to high levels of magnetic activity.

**Key words:** *binaries: eclipsing – stars: individual: NGC2204-S892 – stars: low-mass – stars: K-type*

## 1 Introduction

Significant discrepancies are known to exist on the lower main sequence (LMS) between theoretical predictions and the actual parameters of stars. For stars in the 0.2-0.8  $M_\odot$  mass range observed radii are larger by up to 10 – 15 percent, and effective temperatures lower by several percent than predicted by theory. According to Morales, Ribas, & Jordi (2008), “... current stellar structure and evolution models are not adequate to describe the physical (radii) and radiative (effective temperature, color indices) properties of... low-mass stars. The problem is particularly severe for the analysis of open clusters or star forming regions”. Indeed, LMS stars (LMSS) appear 50 – 90 percent older or younger in mass-radius diagrams than they really are, depending on whether post- or pre-MS models are used (Stassun et al. 2009). No definitive explanation for the inflated radii of LMSS has yet been given, but mounting evidence suggests that they result from intense magnetic activity associated with high spot-coverage

---

\*Based on photometric observations performed at CTIO, LCO and SAAO, and spectroscopic data collected with the Very Large Telescope at ESO Paranal Observatory under programme 382.D-0439(A).

(Chabrier *et al.* 2007; Ribas *et al.* 2008; Morales *et al.* 2008). A positive correlation between radius and activity level was found for a few members of close binaries by López-Morales (2007). This important discovery clearly deserves further study, extending it onto a larger region of parameter space.

Active low-mass stars are fast rotators with rotation periods shorter than  $\sim 3$  days, and their activity is strongly correlated with rotational velocity (*e.g.*, Mohanty & Basri 2003). It is evident, then, that the best objects with which to study the dependence of radius on activity are members of close eclipsing binary systems. First, their masses and radii can be accurately determined from photometric and spectroscopic data. Second, they are rotationally synchronized, and due to the spread in orbital periods they should exhibit a wide range of activity. Unfortunately, LMS binaries are very rare: according to Shaw & López-Morales (2007), there is only one such system per about million stars listed in recent sky surveys; whereas Ribas *et al.* (2008) mention only 7 binaries for which masses and radii have been derived with uncertainties below 3 percent. The situation may improve owing to future large-area synoptic surveys like SDSS II, Pan-STARRS and LSST (Blake *et al.* 2008), but at the moment every new LMS binary with components in the mass range  $0.2 M_{\odot} < m < 0.8 M_{\odot}$  is highly valuable as a potential source of data enabling detailed studies of the effects of magnetic activity on stellar structure and evolution.

It should be mentioned here that optical interferometry has recently enabled accurate direct measurements of the radii of nearby LMSS. However, the masses are not directly measurable in this case, and can only be estimated through comparison with empirical mass-luminosity relations or other indirect methods. Moreover, interferometric measurements are limited to single stars whose rotational velocities rarely exceed  $3 \text{ km s}^{-1}$ , implying a low activity or lack thereof. Not surprisingly, the radii of single M dwarfs measured by interferometry do not show obvious excesses, and within observational errors they are compatible with models (Demory *et al.* 2009). Those authors detected possibly meaningful deviations only for early K stars, and found them to disappear when the mixing length parameter  $l_{\text{mix}}/H_P$  of 1.5–1.9 is used instead of 1.0.

In the present paper we analyze NGC2204-S892 – a newly discovered detached double-lined eclipsing binary composed of two late K dwarfs (hereafter: S892). The binary is a foreground object in the field of the open cluster NGC 2204, originally described by Rozyczka *et al.* (2007) as star #892. They reported orbital period of slightly less than 0.5 d with brightness varying between  $V \approx 17.4$  mag at maximum and  $V \approx 18.4$  mag at primary minimum, and secondary minimum  $\sim 0.55$  mag deep. Based on the dereddened  $B-V$  color and the difference between the depths of the minima, they estimated  $\sim 0.6 M_{\odot}$  for the mass of the primary.

In 2008 we collected 5 light curves of S892 (3 in  $V$ , 1 in  $B$  and 1 in  $I$ ) and derived an orbital period of  $0.451780 \pm 0.000001$  d. We also obtained 20 UVES spectra enabling accurate measurements of the radial velocity amplitudes ( $145 \pm 2 \text{ km s}^{-1}$  and  $165 \pm 2 \text{ km s}^{-1}$  for primary and secondary, respectively). The details of our observing runs are provided in Section 2. Section 3 presents the analysis of the collected data and the resulting physical parameters of the binary. The properties of the binary are discussed in Section 4 in relation to the discrepancies between empirical and theoretical mass-radius relations for LMSS, and a brief summary of our work is presented in Section 5.

## 2 Observations

S892 is located in Canis Major at  $\alpha_{2000} = 06^{\text{h}}15^{\text{m}}55^{\text{s}}.42$  and  $\delta_{2000} = -18^{\circ}44'51''.7$ . We observed it for a week in January 2008 with the 2.5-m Irénée du Pont telescope at Las Campanas Observatory (LCO), for another week in November 2008 with the 1.0-m Yale telescope at Cerro Tololo Interamerican Observatory (CTIO), and for 2 weeks in December 2008 with the 1.0-m Elisabeth telescope at the South African Astronomical Observatory (SAAO). The observations were made in Johnson  $B$  and  $V$ , and Cousins  $I$  bands, yielding a total of 1282 frames. A journal of the observations is given in Table 1 together with numbers of measurements obtained in each run and filter. The spectra of the system were taken between early October 2008 and mid-January 2009 with the UVES spectrograph at VLT UT2 (Kueyen) at the ESO Paranal Observatory under programme 382.D-0439(A).

Table 1: Journal of photometric observations

Site	Observing period	Filters	No. of frames
LCO (2.5m)	11.01-17.01.2008	$B/V$	85/237
CTIO (1.0m)	05.11-13.11.2008	$V$	464
SAAO (1.0m)	03.12-16.12.2008	$V/I$	331/193

### 2.1 Photometry

#### 2.1.1 LCO

Images were taken in the  $B$  and  $V$  bands with the TEK5 camera on the 2.5-m Irénée du Pont telescope at a scale of 0.259 arcsec/pixel. The FoV was  $8.8 \times 8.8$  arcmin<sup>2</sup>, and exposure times ranged from 50 to 120 s in  $V$  and from 120 to 180 s in  $B$ . In a total of  $\sim 17.5$  hours of monitoring time 85 frames in  $B$  and 237 in  $V$  were collected. All  $B$  frames and 235 of the  $V$  frames were useful. The PSF had a FWHM ranging from 0.7 to 2.3 arcsec in  $B$  and from 0.6 to 2.2 arcsec in  $V$ , with median values of 1.1 and 1.0 arcsec, respectively.

#### 2.1.2 CTIO

Images were taken with the Y4K camera on the Yale 1.0-m telescope in  $V$  band only, at a scale of 0.289 arcsec/pixel. The FoV was  $19.7 \times 19.7$  arcmin<sup>2</sup>, and every frame was exposed for 100 s. In a total of  $\sim 41$  hours of monitoring time 464 frames were collected, 459 of which were useful. Only the FoV quadrant containing the binary was processed through the reduction pipeline. In this quadrant the PSF had a FWHM ranging from 1.1 to 2.2 arcsec, with a median of 1.6 arcsec.

#### 2.1.3 SAAO

Images were taken in the  $V$  and  $I$  bands with the STE4 camera on the 1.0-m Elisabeth telescope at a scale of 0.31 arcsec/pixel. The FoV was  $5.3 \times 5.3$  arcmin<sup>2</sup>, and exposure times ranged from 100 to 200 s in  $V$  and from 70 to 150 s in  $I$ . In a total of  $\sim 37$  hours of monitoring time 331 frames in  $V$  and 193 in  $I$  were collected, out of which 322 and 181 were useful, respectively. The seeing was generally poor, and the resulting PSF had a FWHM ranging from

1.3 to 3.6 arcsec in  $V$  and from 1.2 to 3.3 arcsec in  $I$ , with median values of 2.3 and 1.9 arcsec, respectively.

#### 2.1.4 Data reduction

The preliminary processing of the raw data was performed under IRAF<sup>†</sup>. All frames were de-biased and flat-fielded with median-averaged sky flats. The photometry was performed with the DAOPHOT/ALLSTAR package (Stetson 1987). The reduction procedure started from the identification of stars with the subroutine FIND, followed by aperture photometry with the subroutine PHOT. A PSF varying quadratically with  $(x,y)$  coordinates was then constructed for each frame based on 30-40 isolated stars, and used for profile photometry with the ALLSTAR subroutine. The images were inspected visually, and for each camera and each filter one of the best frames was chosen as a template. Instrumental magnitudes of template stars were transformed to the standard system using the data of Kassis *et al.* (1997) available in the WEBDA database. For each frame taken with the same camera and filter the template stars were identified by means of transformations of  $(x,y)$  coordinates, and ALLSTAR photometry for those frames was transformed to the standard system with the template serving as an intermediary. The quality of the transformation was verified by plotting the light curve of a comparison star with similar colors which was located close to S892 in the frames: it did not show any secular trend or discontinuity. The mean  $V$ -band magnitude of that comparison star calculated from all 2008 observations was  $V_{\text{comp}} = 17.627$  mag. The rms deviation from  $V_{\text{comp}}$  was 0.006, 0.017 and 0.016 mag for LCO, CTIO and SAAO data, respectively, and in all cases it was practically equal to the mean error of the photometry calculated by DAOPHOT. The corresponding mean magnitudes obtained from the three sets of data differed from  $V_{\text{comp}}$  by less than  $10^{-3}$  mag.

Based on all 2008 data in the  $V$ -band we derived the following ephemeris of the system:

$$\begin{aligned} t_0 &= \text{HJD } 2454480.6326 \pm 0.0001 \\ P &= 0.451780 \pm 0.000001 \text{ d} \end{aligned} \quad (1)$$

The resulting phased  $V$ -band light curves are shown in Fig. 1. Their variability can be immediately seen by comparing the LCO curve with any of the remaining two. Even the CTIO and SAAO curves differ noticeably, although they are separated by just one month in time.

## 2.2 Spectroscopy

UVES spectra of S892 were obtained in service mode on 10 nights spaced irregularly between 03.10.2008 and 18.01.2009. We used the red arm of the spectrograph in a standard setting centered at  $5800\text{\AA}$  with the detectors binned  $2 \times 2$ . S892 is rather faint, but its short orbital period sets stringent limits on the exposure time (long exposures would blur all spectral features). To keep both  $S/N$  and effective resolution as high as possible we chose a  $t_{\text{exp}}$  of 1200 s (*i.e.*, 3% of the orbital period). In practice two spectra exposed for 600 s each were taken one after another, and combined during data reduction. Such a procedure yielded an average  $S/N \approx 18$  in the reduced spectra, and also facilitated the removal of cosmic rays.

---

<sup>†</sup>IRAF is distributed by the National Optical Astronomy Observatories, which are operated by the AURA, Inc., under cooperative agreement with the NSF.

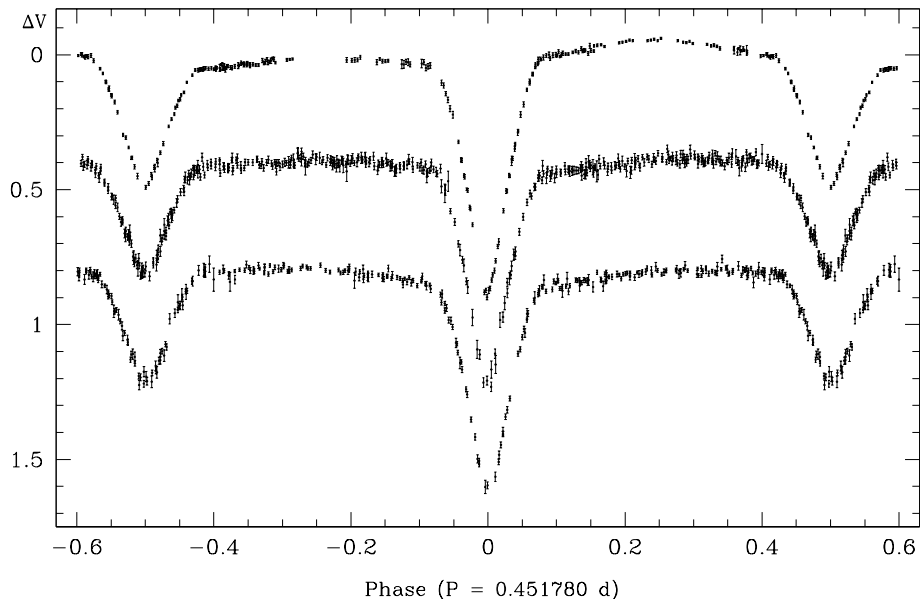


Figure 1: Phased V-band light curves obtained at (from top to bottom): LCO, CTIO and SAAO. The errors, with mean values of 0.007, 0.017 and 0.014 mag, respectively, are calculated by DAOPHOT. The zero-point on the vertical axis corresponds to 17.5 mag, and the curves are displaced from one another by 0.4 mag.

On every observing night four 600 s exposures of S892 were taken in the following sequence: exposure, ThAr calibration spectrum, exposure, flat-field image, exposure, ThAr calibration spectrum, exposure, flat-field image. Each spectrum was delivered in two segments recorded by independent CCD's: the “blue” one extending from 4780 to 5755Å and the “red” one extending from 5835 to 6800Å. We obtained 20 blue and 20 red spectra altogether, at orbital phases between 0.18 and 0.97, with most of them grouped around quadratures. The reduction of the data was performed under IRAF. The raw frames were debiased and flatfielded, and the spectra were extracted and calibrated with the help of NOAO, IMRED and ECHELLE packages.

Radial velocity measurements were based on the broadening function (BF) formalism discussed by Rucinski (2002). The main cause of line broadening in S892 is fast rotation of the components, contributions from other factors are practically negligible. For a rigidly rotating spherical star we have

$$\text{BF}_{rot}(v) = A \left[ (1 - \beta) \sqrt{1 - a^2} + \frac{\pi}{4} \beta (1 - a^2) \right] \quad (2)$$

$$\text{with } a = \frac{v - v_{rad}}{v_{rot} \sin i},$$

where  $\text{BF}_{rot}$  is the rotational BF,  $v_{rad}$  and  $v_{rot}$  are, respectively, radial and rotational velocity,  $\beta$  is the coefficient of linear limb darkening, and  $A$  is an amplitude. The observed BFs were extracted separately from blue and red segments of all spectra, using the spectrum of K5V star HD 10361 from the UVES library as a template. Model BFs used for our analysis were convolutions of two rotational BFs given by equation (2) and a Gaussian with a standard deviation of 40 km s<sup>-1</sup>. Fits to the observed BFs were performed by means of nonlinear

Table 2: Radial velocities.

HJD-2454000	Phase	$v_1$ [km s <sup>-1</sup> ]	$v_2$ [km s <sup>-1</sup> ]
742.8072	0.3146	-131.6 ± 2.0	149.4 ± 0.9
742.8239	0.3518	-117.1 ± 4.2	132.7 ± 6.7
744.7988	0.7231	145.6 ± 0.4	-155.5 ± 5.5
744.8155	0.7600	149.0 ± 2.6	-157.7 ± 4.4
746.8112	0.1774	-128.4 ± 5.7	145.7 ± 6.3
746.8279	0.2144	-141.5 ± 2.1	159.5 ± 0.4
773.7041	0.7041	140.4 ± 1.4	-151.9 ± 10.9
773.7167	0.7319	148.5 ± 3.6	-156.1 ± 9.9
775.7511	0.2351	-141.8 ± 1.4	158.6 ± 5.2
775.7679	0.2722	-142.6 ± 3.5	159.2 ± 5.0
792.7760	0.9191	73.6 ± 0.2	-73.0 ± 1.8
792.7928	0.9562	48.3 ± 2.8	-54.8 ± 5.2
793.8002	0.1860	-132.9 ± 4.4	151.6 ± 4.5
793.8169	0.2230	-142.2 ± 3.9	160.9 ± 5.6
796.7807	0.7832	146.6 ± 6.8	-161.8 ± 5.3
796.7974	0.8202	138.9 ± 0.5	-145.5 ± 4.9
798.6566	0.9354	60.4 ± 1.6	-66.3 ± 1.7
798.6737	0.9734	40.6 ± 0.9	-30.7 ± 7.8
849.5991	0.6950	140.6 ± 1.4	-151.2 ± 8.9
849.6159	0.7323	148.9 ± 0.1	-160.0 ± 12.6

Barycentric radial velocities of S892 measured from the UVES data and phased according to the ephemeris given by equation (1).

least-squares procedures from the GNU Scientific Library. The resulting radial velocities listed in Table 2 are averages from  $v_{\text{blue}}$  and  $v_{\text{red}}$ , *i.e.*, fits to blue and red segment of the spectrum (the errors are estimated from the formula  $\sigma_v = |v_{\text{blue}} - v_{\text{red}}|/\sqrt{2}$ ). As a by-product we obtained projected rotational velocities of both components of the S892 system:  $v_1 \sin i = 79.2 \pm 5.9$  km s<sup>-1</sup> for the primary and  $v_2 \sin i = 76.2 \pm 8.8$  km s<sup>-1</sup> for the secondary. We note that the accuracy of the velocity measurements is degraded by noticeable distortions of the observed BFs due to stellar spots. Not surprisingly, the observational errors are significantly and systematically larger for the secondary component whose lines are weaker and more difficult to measure.

### 3 Modeling

We modeled the S892 system using the PHOEBE interface (Prša & Zwitter 2005) to the Wilson-Devinney code (Wilson & Devinney 1971). Because the narrow eclipses in Fig. 1 indicate that the components of the binary are far from contact, a detached configuration was adopted for all calculations. However, since the orbital period of S892 is rather short, and its light curves suggest that both components are nonspherical, we also included proximity effects for the primary and secondary. The bolometric albedo was kept fixed at 0.5, which is the standard value for stars with convective envelopes, and we enabled the double reflection option. For the limb darkening a logarithmic law was used as implemented in PHOEBE 0.31a. In all calculations the gravity brightening coefficient  $\beta_1$  was set to 0.32 – the classical value obtained by Lucy (1967). To check the sensitivity of the results to that parameter, a few converged fits were re-run with  $\beta_1 = 0.2$  – a value obtained by Claret (2000). Changes, if any, were of the same order as the accuracy of the fit.

As there was no indication for nonzero eccentricity in any of our five light curves, we set  $e \equiv 0$ . The period was adopted from the photometric data. Both components were assumed to be entirely synchronized, *i.e.*, their synchronicity parameters were set to 1.0. Having no clues about the chemical composition of S892 we assumed that it has solar metallicity. Rozycka *et al.* (2007) estimated that the system is located not more than  $\sim 1$  kpc away from the Sun and  $\sim 250$  pc below the Galactic plane, so that it most probably belongs to the thin disk population, and its true metallicity should not differ much from the assumed value. We re-ran a few converged fits with  $[\text{Fe}/\text{H}] = -0.5$  and  $[\text{Fe}/\text{H}] = 0.5$ . No significant changes were found compared to the case with  $[\text{Fe}/\text{H}] = 0$ .

The estimates of Rozycka *et al.* (2007) were used as the initial guess for the masses of the components. Based on masses and period, we obtained an estimate of the semimajor axis  $a$  of the system. An initial guess for the inclination  $i$  was provided by a preliminary fit to the SAAO  $V$ -band curve, which was the most symmetric one among the three. A preliminary fit to the velocity curve in turn yielded updated (*i.e.*, compatible with  $i$ ) approximations for masses and  $a$ . We checked that keeping  $T_1$  at a value fixed between 4100 K and 4300 K does not significantly influence the outcome of iterations for any parameter of the system except  $T_2$ , and based on our approximate value of  $m_1 = 0.75 M_\odot$  we adopted  $T_1 = 4200$  K – in agreement with  $T_2 = 4220 \pm 150$  K obtained by Torres & Ribas (2002) for the secondary component of V818 Tau with  $m_2 = 0.76$  or  $T_2 = 4200 \pm 200$  K obtained by Bayless & Orosz (2006) for both components of 2MASS J05162881+2607387 with  $m_1 = 0.79$  and  $m_2 = 0.77 M_\odot$ .

Because of the evident variability of the light curve (see Fig. 1) we could not use the photometric data en bloc. Instead, we adopted the following procedure:

1. Choose one of LCO, CTIO or SAAO photometric data sets.
2. Keeping  $a$  and mass ratio  $q \equiv m_2/m_1$  fixed, make a fit to the light curve by iterating for  $T_2$ ,  $i$ , primary's luminosity  $L_1$  and surface potentials of both components. Add spots to account for the asymmetries of light curves. The result will serve as the *base fit* for the next steps of the procedure.
3. Fix all parameters of the base fit except  $a$  and  $q$ . Make a fit to the velocity curve by iterating for  $a$  and  $q$ .
4. Go to (2). Repeat steps (2) – (4) until the base fit converges upon completing (2). We consider the fit converged when stellar radii  $R_1$  and  $R_2$  change by less than  $0.01 R_\odot$  during one iteration step.
5. Fix all parameters of the converged base fit. Substitute the first photometric data set with one of the remaining two. Adjust number, location and parameters of spots until photometric residua do not show any systematic or large-scale variability in phase.
6. Relax  $a$  and  $q$ . Make a fit to the velocity curve.
7. Fix  $a$  and  $q$ . Relax the remaining parameters, and make a fit to the photometric data.
8. Go to (6). Repeat steps (6) – (8) until upon completing (7) the fit converges according to the same criterion as in (4).
9. Repeat steps (5) – (8) for the third set of photometric data.
10. Repeat steps (2) – (8) using another set of photometric data to obtain the base fit.
11. Repeat steps (2) – (8) using the last set of photometric data to obtain the base fit.

An example result of fitting is shown in Fig. 2, with observational points omitted for clarity. In this case the base fit was obtained from the LCO data. The rms residual  $V$  magnitude of LCO, CTIO and SAAO data is equal to 0.007, 0.017 and 0.016 mag, respectively; *i.e.*, it is practically the same as the accuracy of photometric measurements reported in Section 2.1.4. The rms residual  $B$  and  $I$  magnitudes amount to 0.014 and 0.017 mag, respectively. Note that all  $V$ -band light curves in Fig. 2 are asymmetric (the same holds for the  $B$ - and  $I$ -band light curves). The proximity effect is clearly visible in the “de-spotted” light curves (dotted lines in Fig. 2), indicating a significant tidal distortion of the components of S892.

The number of spots placed on model stars to match the photometric data varied from 1 to 5 per star in different fits. Both dark and bright spots were introduced, with  $|\Delta T_{\text{eff}}|/T_{\text{eff}}$  ranging from 0.01 to 0.06. In most cases the spot

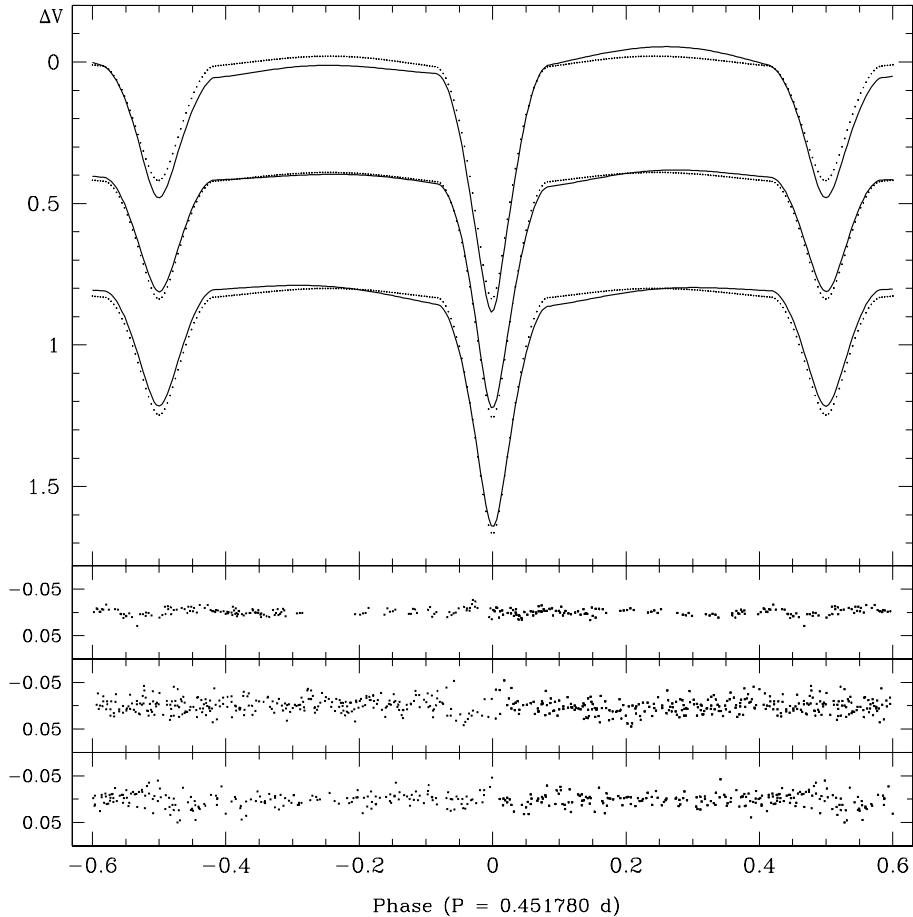


Figure 2: Upper panel: example fits to  $V$ -band light curves phased with  $P = 0.451280$  d (solid lines). Dotted lines: the same fits shown after the spots have been removed from both components of the system. From top to bottom: LCO, CTIO and SAAO. The zero-point on the vertical axis corresponds to  $V = 17.5$  mag, and the curves are displaced from one another by 0.4 mag. Lower panels: residuals from fits with spots. From top to bottom: LCO, CTIO and SAAO. The base fit (see text for explanations) was obtained from LCO data.



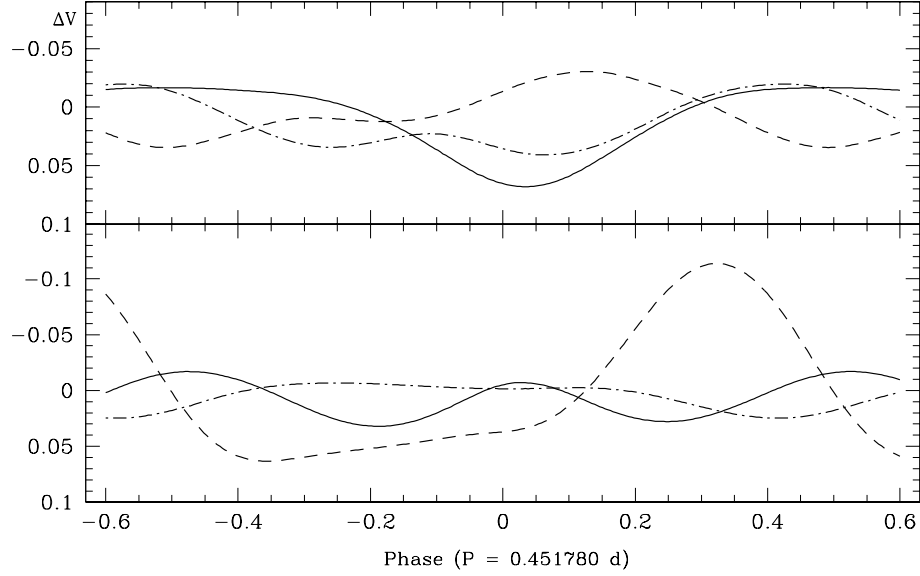


Figure 3: Example modulations of  $V$ -band magnitude due to spots on primary and secondary component of S892 (upper and lower panel, respectively). Dashed, dash-dotted and solid lines: fits to LCO, CTIO and SAAO light curves.

coverage was rather high – between 0.3 and 0.5 of the whole surface of the star. As the adopted configuration of spots is not unique we do not think it worthwhile to go into details, and we limit ourselves to just one example illustrated in Fig. 3 which shows periodic variations in the  $V$ -band caused solely by the presence of spots (*i.e.*, without the effect of ellipticity). The data for Fig. 3 are taken from models for which the base fit was obtained from the LCO photometry.

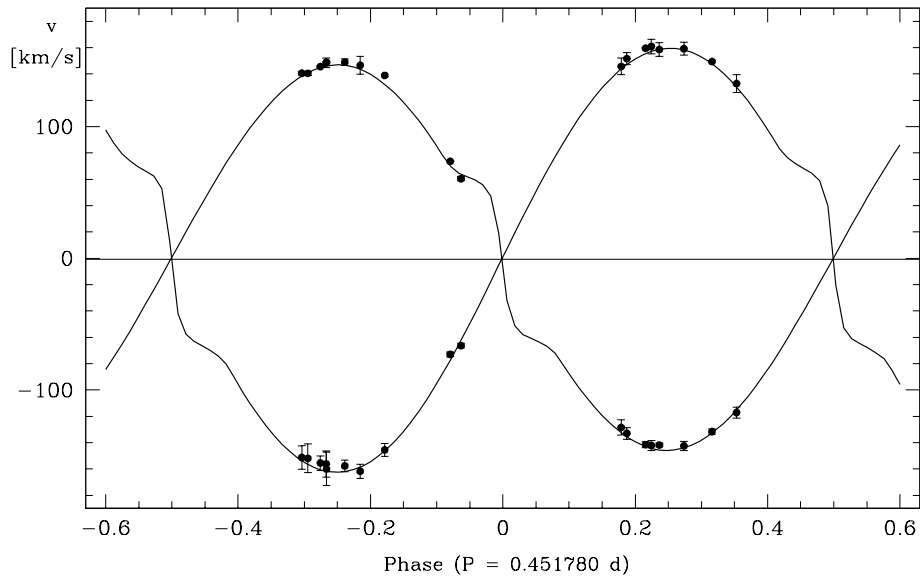


Figure 4: Example fit to UVES velocity data. The horizontal line shows the systemic velocity of  $-0.8 \pm 0.4 \text{ km s}^{-1}$ .

An example velocity fit for phases  $\phi < 0.9$  is shown in Fig. 4 (bends on the synthetic curve are due to the Rossiter - McLaughlin effect). We decided to not include points with  $\phi > 0.95$  despite their formal errors in Table 2 being rather small because we suspected that heavy line-blending in the corresponding spectra would introduce unaccountable systematic deviations. Indeed, after a few trial fits with all velocity points taken into account we found that for  $\phi > 0.95$  it was impossible to get residual velocities smaller than  $10 \text{ km s}^{-1}$ , whereas the rms residual velocity for  $\phi < 0.9$  was equal to only  $2.1 \text{ km s}^{-1}$ .

Table 3: Physical parameters of S892

$P$	[d]	0.451780	$\pm 0.000001$	
$a$	$[R_{\odot}]$	2.77	$\pm 0.01$	$(\begin{smallmatrix} +0.013 \\ -0.015 \end{smallmatrix})$
$e$	(fixed)	0.		
$i$	[degrees]	85.36	$\pm 0.28$	$(\begin{smallmatrix} +0.58 \\ -0.24 \end{smallmatrix})$
$\gamma$	$[\text{km s}^{-1}]$	-0.8	$\pm 0.4$	
$m_1$	$[M_{\odot}]$	0.733	$\pm 0.005$	$(\begin{smallmatrix} +0.011 \\ -0.007 \end{smallmatrix})$
$m_2$	$[M_{\odot}]$	0.662	$\pm 0.005$	$(\begin{smallmatrix} +0.012 \\ -0.008 \end{smallmatrix})$
$R_1$	$[R_{\odot}]$	0.719	$\pm 0.014$	$(\begin{smallmatrix} +0.030 \\ -0.017 \end{smallmatrix})$
$R_2$	$[R_{\odot}]$	0.680	$\pm 0.017$	$(\begin{smallmatrix} +0.031 \\ -0.014 \end{smallmatrix})$
$T_1$	[K] (fixed)	4200		
$T_2$	[K]	3940	$\pm 20$	$(\begin{smallmatrix} +110 \\ -100 \end{smallmatrix})$
$M_{\text{bol}1}$	[mag]	6.89	$\pm 0.04$	$(\begin{smallmatrix} -0.20 \\ +0.15 \end{smallmatrix})$
$M_{\text{bol}2}$	[mag]	7.29	$\pm 0.04$	$(\begin{smallmatrix} -0.20 \\ +0.16 \end{smallmatrix})$

3<sup>rd</sup> column: rms deviations from mean values obtained in 9 fits to light and velocity curves.  
 4<sup>th</sup> column above the horizontal line: largest deviations from the mean; below the horizontal line: variations corresponding to  $\pm 100 \text{ K}$  change in  $T_1$

All fits made according to the procedure described above produced 9 sets of system parameters whose averaged values are listed in Table 3 together with rms deviations from the nine-fit mean (since the "de-spotting" procedure may in principle introduce systematic errors, we also give the largest deviations from the mean). Obviously, both the mean values and the errors might change if we had more light curves. Unfortunately, a significant improvement of their accuracy would require at least  $\sim 10$  additional light curves at epochs separated by at least several weeks. Note that temperatures – and, obviously, the bolometric magnitudes they yield – are not well constrained by the data (see Section 4). Their errors in column 3 of Table 3 are but formal results of the fits with  $T_1 = 4200 \text{ K}$ ; depending on the exact value of  $T_1$  they may vary as indicated in the last column.

To check the influence of photometry errors on values given in Table 3 we removed spot effects from our best (LCO) and poorest (CTIO) data, and performed extensive (10000 points) Monte Carlo fitting with the help of the JK-TEBOP code (Southworth *et al.* 2007). For the LCO light curve the errors of  $R_1$  and  $R_2$  were equal to  $0.0021 R_{\odot}$  and  $0.0026 R_{\odot}$ , respectively, while for the CTIO light curve they amounted to  $0.0075 R_{\odot}$  and  $0.0090 R_{\odot}$ . Since photometry errors  $\sigma_{\text{ph}}$  and "de-spotting" errors  $\sigma_{\text{ds}}$  are independent, the total error may be approximated by the square root of the sum ( $\sigma_{\text{ph}}^2 + \sigma_{\text{ds}}^2$ ). Such an operation causes the errors of  $R_1$  and  $R_2$  to increase, respectively, by 14% and 13% compared to the values given in the 3<sup>rd</sup> column of Table 3.

The radii of the components imply rotational velocities  $v_1 \sin i = 80.8 \pm 1.1 \text{ km s}^{-1}$  and  $v_2 \sin i = 76.3 \pm 2.3 \text{ km s}^{-1}$ , which agree very well with  $v_1 \sin i = 79.2 \pm 5.9 \text{ km s}^{-1}$  and  $v_2 \sin i = 76.2 \pm 8.8 \text{ km s}^{-1}$  derived from BF fits in Sec-

tion 2.2, thus indicating the consistency of our solution. Note also that the low systemic velocity of S892 adds credence to our assumption concerning its metallicity.

## 4 Discussion

Several authors, *e.g.*, Morales *et al.* (2008) and references therein, have found that radii of components of lower main sequence binary stars (LMSS) are systematically and significantly larger than predicted by the theory. Our analysis of S892 confirms this finding. Incidentally, the radii of the components of this system agree very well with the empirical  $R(M)$  relation

$$R/R_{\odot} = 0.0324 + 0.9343M/M_{\odot} + 0.0374(M/M_{\odot})^2 \quad (3)$$

obtained by Bayless & Orosz (2006), which for  $M_1 = 0.733M_{\odot}$  and  $M_2 = 0.662M_{\odot}$  yields  $R_1 = 0.737R_{\odot}$  and  $R_2 = 0.667R_{\odot}$ . The updated  $M$ – $R$  diagram for components of well-surveyed binary LMSS is shown in Fig. 5.

As we already mentioned, based on our data it is impossible to find accurate values of  $T_1$  and  $T_2$ . This is because we cannot derive absolute fluxes or effective temperatures from light and velocity data alone as we do not know the distance to S892 from independent measurements. In principle, we might try to match the spectra of this system to binary spectral templates following Becker *et al.* (2008). However, an additional problem arises here due to large and variable spot coverage of both components. As a consequence, the spectra of the components are intrinsically variable (see Fig. 6), which puts any matching attempts in question. Some changes in Fig. 6 are due to orbital motion; however most of them (*e.g.*, at  $5460 < \lambda[\text{\AA}] < 5480$ ,  $5530 < \lambda[\text{\AA}] < 5590$  and  $\lambda[\text{\AA}] > 5600$ ) result from the intrinsic variability of the components.

Another consequence of the vigorous activity of S892 is strong variability of the light curve, as illustrated in Fig. 7. One can see that at some orbital phases the luminosity of the system may vary by almost 10% within a year (note that apparent phase shifts in Fig. 7 are solely due to asymmetries of the light curves). Yet another aspect of the activity is strongly variable  $H\alpha$  emission from both components, with the equivalent width of the line changing within a few weeks from practically 0 to  $\sim 7\text{\AA}$  per component (Fig. 8).  $H\beta$  is also seen in emission, with the equivalent width reaching up to  $\sim 3.5\text{\AA}$ . Neither  $H\alpha$  nor  $H\beta$  are ever seen in absorption. We were not able to detect any secular or periodic intensity changes of either line, and we concluded that the hydrogen emission seems to be entirely chaotic.

A system like this should be a fairly strong source of X-rays. Based on the relation between radius and  $L_X/L_{\text{bol}}$  found by López-Morales (2007) we can expect the total X-ray luminosity of S892 to reach  $\sim 5 \times 10^{29} \text{ erg s}^{-1}$ . Unfortunately, because of the large distance of the system from the Sun the expected flux ( $\sim 5 \times 10^{-15} \text{ erg cm}^{-2} \text{ s}^{-1}$ ) is far too low to be registered in the ROSAT all-sky survey. We did not find relevant X-ray data in other catalogs or databases, either. An attempt to estimate the age of S892 based on the equivalent width of the Li I  $\lambda 6708$  line was also futile – the line could not be detected. The quality of our spectra is insufficient to draw any firm conclusion from this negative result – we can only say that the system almost certainly is not very young. Finally, we searched for proper motion data. S892 is listed in the UCAC3 Catalogue (Finch *et al.* 2009) as 3UC143-028414, with  $\mu_{\alpha} = -7.6 \text{ mas yr}^{-1}$  and

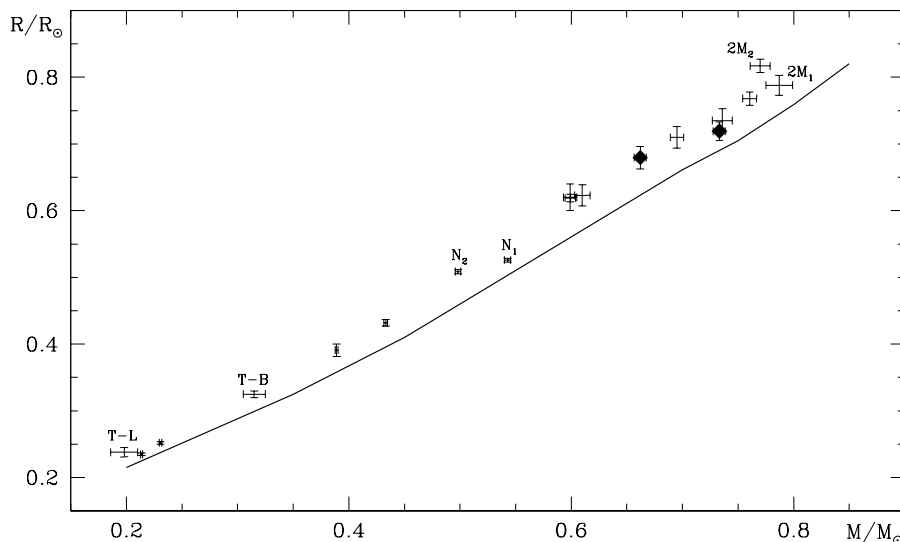


Figure 5: Mass-Radius diagram for low-mass eclipsing binary stars with observationally determined parameters (only stars with uncertainties below 3% both in mass and radius are included). The components of S892 are indicated by diamonds. The solid line is a theoretical 1.0 Gyr isochrone based on the solar composition models of Baraffe et al. (1998). The data for NSVS 01031772 (marked with  $N_{1,2}$ ), 2MASS J05162881+2607387 (marked with  $2M_{1,2}$ ), T-Boo0-00080 (marked with T-B) and T-Lyr1-01662 (marked with T-L) are taken, respectively, from López-Morales et al. (2006), Bayless & Orosz (2006) and Fernandez *et al.* (2009). All remaining data (from left to right for CM Dra B, CM Dra A, CU Cnc B, CU Cnc A, GU Boo B, YY Gem AB, GU Boo A, RXJ0239.1-1028 B, RXJ0239.1-1028 A and V818 Tau B) are taken from Ribas (2006).

$\mu_\delta = -3.8 \text{ mas yr}^{-1}$ , but large errors ( $6.4 \text{ mas yr}^{-1}$  in both coordinates) make this information rather uninteresting.

Based on composite  $\text{CaH}_2$ ,  $\text{CaH}_3$  and  $\text{TiO}_5$  molecular indices, Becker et al. (2008) derived  $T_{\text{eff}} = 3730 \pm 100 \text{ K}$  for the  $M = 0.66 M_\odot$  primary component of 2MASS J01542930+0053266. While this result marginally agrees with our  $T_2$ ,<sup>‡</sup> it is tempting to verify it using an additional evidence. Unfortunately, the indices used by Becker et al. (2008) are defined for  $\lambda > 6800 \text{ \AA}$  (Reid, Hawley & Gizis 1995), *i.e.*, for wavelengths longer than the red limit of our spectra. Not being able to apply their method to our data, we compared their result to temperatures of similar systems reported in the literature.

To our surprise, both stars in YY Gem and both stars in GU Boo, all being by  $\sim 10\%$  less massive than the primary of 2MASS J01542930+0053266 were found to be by up to 350 K *hotter* (Torres & Ribas 2002; López-Morales & Ribas 2005). Active stars in this mass range are known to be cooler than nonactive ones (see Section 1), but in all three systems the level of activity is similar (in principle, in 2MASS J01542930+0053266 it should be even lower than in the remaining two because of a relatively long orbital period). Adopting  $T_2 = 3730 \text{ K}$  for our secondary and using the flux ratio obtained from our fits, we obtain for our  $0.73 M_\odot$  primary  $T_1 = 3940 \text{ K}$  – a value assigned by López-Morales & Ribas (2005) to GU Boo A, whose mass is smaller by almost 20%. We conclude that

<sup>‡</sup>Note that the larger error margin from the 4<sup>th</sup> column of Table 3 should be applied here.

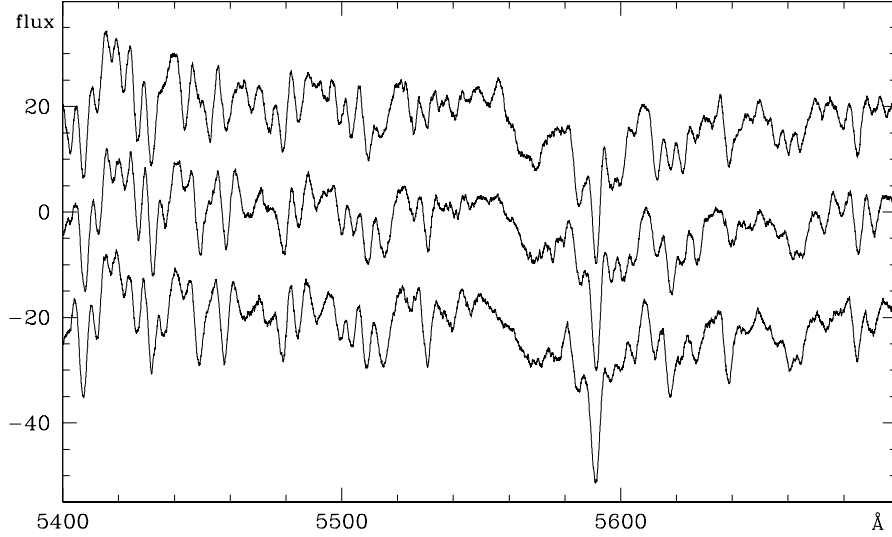


Figure 6: An illustration of the spectral variability of S892. From top to bottom: spectra obtained on HJD 2454746 ( $\phi=0.177$ ), HJD 2454849 ( $\phi=0.695$ ) and HJD 2454744 ( $\phi=0.723$ ). The flux scale is arbitrary; the top and bottom spectra are displaced vertically by 20 units.

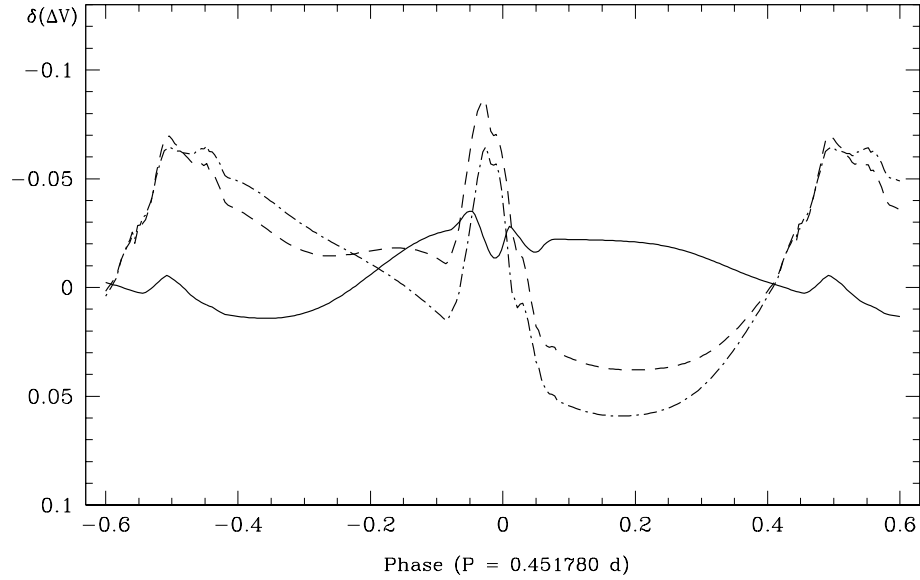


Figure 7: Variability of the V-band light curve illustrated by differences between solid curves from Fig. 2. Dashed: CTIO-LCO; dash-dotted: SAAO-LCO; solid: CTIO-SAAO.

3940 K from Table 3 is a fairly realistic value of  $T_2$  in the S892 system. Note that while all these discrepancies provide a good illustration of the notorious problem with temperature measurements, they luckily do not influence our main findings.

Bolometric corrections  $BC_1 = -1.00$  mag and  $BC_2 = -1.25$  mag (Bessell, Castelli & Plez 1998) translate our  $M_{\text{bol}1}$  and  $M_{\text{bol}2}$  into  $M_{V1} = 7.89$  mag and

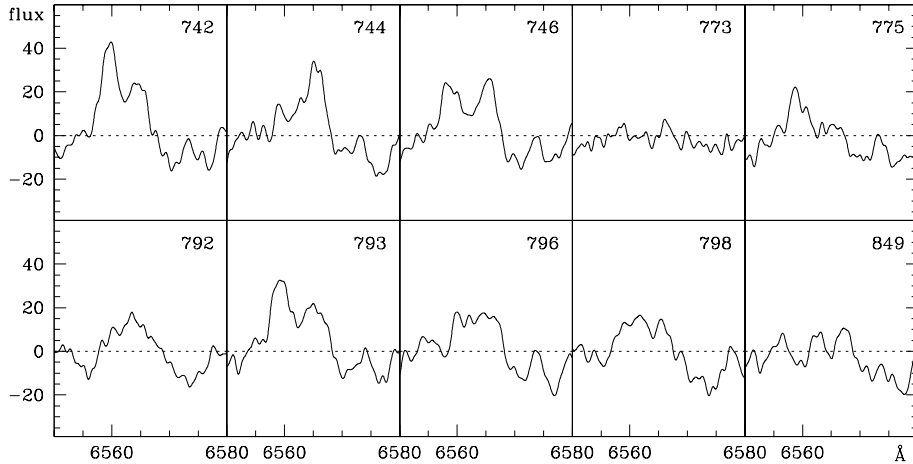


Figure 8:  $H\alpha$  emission in S892. The equivalent width of the line varies from 0 to  $\sim 7\text{\AA}$  per component. The number in the upper right corner of each frame indicates the date of observation, in HJD-2454000.

$M_{V2}=8.54$  mag, resulting in a combined absolute  $V$ -band magnitude of 7.41 mag at the phase of maximum light. NGC2204 is  $\sim 4$  kpc distant (Kassis *et al.* 1997) and only weakly reddened, with  $E(B-V)\approx 0.1$  (Schlegel *et al.* 1998) and  $A_V\approx 0.32$ . Thus, the revised distance to S892 is about 1050 pc if the whole absorbing material is located behind the system, and about 900 pc if it is located in front of it.

## 5 Conclusions

We discovered and analyzed a detached eclipsing binary composed of two late K dwarfs. Based on light and velocity curves we derived orbital period of  $0.451780\pm 0.000001$  d, semimajor axis  $a=2.77\pm 0.01 R_\odot$  and inclination  $i=85^\circ 36\pm 0^\circ 28$ . The masses of the components ( $M_1=0.733\pm 0.005 M_\odot$ ;  $M_2=0.662\pm 0.005 M_\odot$ ) and their radii ( $R_1=0.72\pm 0.01 R_\odot$ ;  $R_2=0.68\pm 0.02 R_\odot$ ) are consistent with the empirical mass-radius relationship established recently for LMSS in binary systems by Bayless & Orosz (2006): both stars are larger and cooler compared to theoretical models.

The discrepancy between theory and observations was originally thought to arise from inaccuracies in the equation of state and/or opacity. It turned out, however, that models based on the same physics were entirely compatible with observed properties of single stars or stars in wide binaries (López-Morales *et al.* 2006). Another approach to the problem was suggested by a positive correlation between radius and activity level found for a few members of close binaries by López-Morales (2007). It was realized that the basic difference between single stars and components of short-period binary systems was high rotational velocities of the latter, promoting high levels of magnetic activity. Strong magnetic fields can inflate the star due to large spot coverage (thus lowering the effective temperature) and/or partial inhibition of convection (which has the same effect as increased opacity; see Chabrier *et al.* for details).

Both components of our binary are very active, showing high spot-coverage, unstable light curves, and strong variability of the emission in hydrogen lines.

Thus, our results support the increasing evidence that the observed inflation of radii of K and M dwarfs is related to high levels of magnetic activity.

**Acknowledgements.** JK, PP, WP and MR were supported by the grant MISTRZ from the Foundation for the Polish Science and by the grant N N203 379936 from the Polish Ministry of Science and Higher Education (PMSHE). MC and PP acknowledge support from Chilean FONDAF Centro de Astrofísica No. 15010003. Support for PP was also provided by the grant N N203 301355 from PMSHE, and MC was also supported by Proyecto Basal PFB-06/2007 and Proyecto FONDECYT Regular #1071002. IBT acknowledges support from NSF grant #0507325. This research made use of the databases SIMBAD (operated at CDS, Strasbourg, France) and WEBDA (operated at the Institute for Astronomy of the University of Vienna). We thank the staff of VLT for the crucial spectroscopic observations, and the referee, Grzegorz Pojmanski, for his constructive remarks.

## REFERENCES

- Baraffe I., Chabrier G., Allard F. and Hauschildt P. H. 1998, *Astron. Astrophys.*, **337**, 403.  
 Bessell M.S., Castelli F. and Plez B. 1998, *Astron. Astrophys.*, **333**, 231.  
 Bayless A.J. and Orosz J.A. 2006, *Astrophys. J.*, **651**, 1155.  
 Becker A.C., Agol E., Silvestri N.M., Bochanski J.J., Laws C., West A.A., Basri G., Belokurov V., Bramich D.M., Carpenter J.M., Challis P., Covey K.R., Cutri R.M., Evans N.W., Fellhauer M., Garg A., Gilmore G., Hewett P., Plavchan P., Schneider D.P., Slesnick C.L., S. Vidrih S., Walkowicz L.M. and Zucker D.B. 2008, *MNRAS*, **386**, 416.  
 Blake C.H., Torres G., Bloom J.S. and Gaudi B.S. 2008, *Astrophys. J.*, **684**, 635.  
 Chabrier, G., Gallardo, J. and Baraffe, I. 2007, *Astron. Astrophys.*, **472**, L17.  
 Claret, A. 2000, *Astron. Astrophys.*, **359**, 289.  
 Demory B.-O., Ségransan D., Forveille T., Queloz D., Beuzit J.-L., Delfosse X., Di Folco E., Kervella P., Le Bouquin J.-B., and Perrier C. 2009, *Astron. Astrophys.*, **505**, 205.  
 Fernandez J.M., Latham D.W., Torres G., Everett M.E., Mandushev G., Charbonneau D., ODonovan F.T., Alonso R., Esquerdo G.A., Hergenrother C.W. and Stefanik R.P. 2009, *Astrophys. J.*, **701**, 764.  
 Finch C.T., Zacharias N., Girard T., Wycoff G. and Zacharias M.I. 2009, *Bull. Am. Ast. Soc.*, **41**, 427.  
 Kassis M., Janes K.A., Friel E.D. and Phelps R.L. 1997, *Astron. J.*, **113**, 1723.  
 López-Morales M. 2007, *Astrophys. J.*, **660**, 732.  
 López-Morales M., Orosz J.A., Shaw J.S., Havelka L., Arévalo M.J., McIntyre T. and Lázaro C. 2006, *astro-ph/06110225*.  
 López-Morales M. and Ribas I. 2005, *Astrophys. J.*, **631**, 1120.  
 Lucy, L. 1967, *Zeitschrift fr Astrophysik*, **6**, 89.  
 Morales J.C., Ribas I. and Jordi C. 2008, *Astron. Astrophys.*, **478**, 507.  
 Mohanty S. and Basri G. 2003, *Astrophys. J.*, **583**, 451.  
 Prša A. and Zwitter T. 2005, *Astron. J.*, **628**, 426.  
 Reid I.N., Hawley S.L. and Gizis J.E. 1995, *Astron. J.*, **110**, 1838.  
 Ribas I. 2006, *Astrophys.Sp.Sci.*, **304**, 89.  
 Ribas I., Morales J.C., Jordi C., Baraffe I., Chabrier G. and Gallardo J. 2008, *Mem.Soc.Astr.It.*, **79**, 562.  
 Rozyczka M., Kaluzny J., Krzeminski W. and Mazur B. 2007, *Acta Astron.*, **57**, 323.  
 Rucinski S.M. 2002, *Astron. J.*, **124**, 1746.  
 Schlegel, D.J., Finkbeiner, D.P. and Davis, M. 1998, *Astrophys. J.*, **500**, 525.  
 Shaw J.S. and López-Morales M. 2007, *ASPC*, **362**, 15.  
 Southworth, J., Bruntt, H. and Buzasi, D. L. 2007, *Astron. Astrophys.*, **467**, 1215.  
 Stassun K.G., Hebb L., López-Morales M. and Prša A. 2009, *IAU Symp*, **258**, 161.  
 Stetson P.B. 1987, *P.A.S.P.*, **99**, 191.  
 Torres G. and Ribas I. 2002, *Astrophys. J.*, **567**, 1140.  
 Wilson R.E. and Devinney E.J. 1971, *Astron. J.*, **166**, 605.